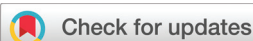


## RESEARCH ARTICLE

[View Article Online](#)  
[View Journal](#) | [View Issue](#)

 Cite this: *Inorg. Chem. Front.*, 2021, **8**, 3096

# A novel Cd-MOF with enhanced thermo-sensitivity: the rational design, synthesis and multipurpose applications†

 Ping Ju, <sup>a</sup> Mengting Li,<sup>a</sup> Hua Yang,<sup>b</sup> Long Jiang,<sup>c</sup> Lian Xia, <sup>a</sup> Rongmei Kong, <sup>a</sup> Ensheng Zhang <sup>\*a</sup> and Fengli Qu <sup>\*a</sup>

A novel fluorescent Cd-MOF probe  $[\text{Cd}_2(\text{btec})(\text{TPB})_{0.5}(\text{H}_2\text{O})_4] \cdot 2\text{H}_2\text{O}$  (complex **1**, TPB = 1,2,4,5-Tetra(4-pyridyl)benzene) has been rationally designed and synthesized, and its multipurpose sensing applications have been revealed. The thermo-sensitive property of complex **1** was investigated in a wide temperature range from 20 °C to 160 °C. A good linear relationship was observed between the fluorescence quenching efficiency of complex **1** and the circumstance temperature, which suggested that complex **1** could be a promising material for application in fluorescent thermometers. Stable suspensions could be obtained after dispersion of complex **1** in various solvents, especially in water. A remarkable red shift (about 20 nm) in the fluorescence emission spectrum of complex **1** was observed when  $\text{H}_2\text{O}$  was used as the dispersion medium compared with that in  $\text{D}_2\text{O}$ , which could be used for distinguishing  $\text{D}_2\text{O}$  from  $\text{H}_2\text{O}$ . Furthermore, based on the strong inner filtering effect (IFE), the fluorescence detection of acetone in water was carried out using complex **1**- $\text{H}_2\text{O}$  suspensions. Real-time fluorescence quenching was observed after the addition of acetone into complex **1**- $\text{H}_2\text{O}$  suspensions. Moreover, the fluorescence quenching efficiency vs. the concentration of acetone fitted well with a non-linear equation ( $R^2 = 0.9929$ ) with an experimental detection limit for acetone as 0.06% (vol%). In addition, the photoelectric responses study revealed that complex **1** might be modified and used as a photoelectric sensor.

Received 8th March 2021,

Accepted 16th April 2021

DOI: 10.1039/d1qi00198a

[rsc.li/frontiers-inorganic](http://rsc.li/frontiers-inorganic)

## 1. Introduction

Luminescent metal-organic frameworks (LMOFs) as promising candidates for the construction of optical sensors have attracted considerable concerns in the past few years.<sup>1–8</sup> To date, various kinds of LMOFs probes for the detection of gases,<sup>1,5,8</sup> explosives,<sup>6,7,9–12</sup> ions<sup>7</sup> and biomolecules<sup>5,13,14</sup> have been fabricated. Due to the numerous ligands, metal ions and coordination modes that could be used in the construction of MOFs, the structural diversity of MOFs has been greatly enhanced. It is not doubtful that more novel MOFs with interesting structural diversity and various potential applications will be revealed in the future. Stimuli-responsive MOFs that

could respond to the disturbance, such as the change of temperature, humidity and mechanical pressure, are attracting comprehensive concerns.<sup>15–19</sup> It is noteworthy that temperature-responsive LMOFs that can be used as promising luminescence thermometers in specific occasions, such as strong electromagnetic field and fluctuating conditions, deserve more attention in the future.<sup>20–24</sup>

According to the literature, flexible LMOFs<sup>16–18</sup> and MOFs that are fabricated with lanthanide metal ions<sup>22–25</sup> may be promising candidates for luminescence thermometers. Flexible MOFs display transformations, such as negative thermal expansion,<sup>26–28</sup> highly anisotropic thermal expansion,<sup>26,29</sup> crystal-to-crystal phase transition<sup>26,30</sup> and thermal amorphization<sup>31,32</sup> when subjected to temperature changes. Dual-emitting LMOFs fabricated with lanthanide metal ions exhibit fluorescent responses to temperature variation.<sup>20,22–25,33</sup> Moreover, the composite of lanthanide-based MOFs with dyes could also afford ratiometric luminescent thermometers.<sup>34,35</sup> Although great progress has been made in the study of temperature-responsive LMOFs, most reported LMOF thermometers were operated at temperatures under 298 K (25 °C, Table S1†) and LMOF thermometers fabricated with main group or other transition metal ions were rarely reported.

<sup>a</sup>College of Chemistry and Chemical Engineering, Qufu Normal University, Qufu, Shandong, 273165, P. R. China. E-mail: sdzes2006@163.com, [jenglquhn@hotmail.com](mailto:jenglquhn@hotmail.com)

<sup>b</sup>Laboratory of New Energy & New Functional Materials, College of Chemistry and Chemical Engineering, Yan'an University, Yan'an, Shaanxi, 716000, P. R. China  
<sup>c</sup>Instrumental Analysis & Research Center, Sun Yat-Sen University, Guangzhou 510275, P. R. China

†Electronic supplementary information (ESI) available. CCDC single number: 2018947. For ESI and crystallographic data in CIF or other electronic format see DOI: 10.1039/d1qi00198a

It is well known that the general mechanism behind aggregation-induced emission (AIE) is the restriction of intramolecular motions, such as intramolecular rotation and vibration.<sup>36,37</sup> In contrast, circumstance temperature changes greatly affect the intramolecular motion of AIE molecules, which will change the radiative/nonradiative decay rate and lead to the fluorescence intensity variation.<sup>38–40</sup> Thus, fluorescence intensity-based LMOF thermometers might be fabricated with AIE ligands and used for highly sensitive temperature sensing. 1,2,4,5-Tetra(4-pyridyl)benzene (TPB), as a fantastic X-shaped tetradentate ligand, exhibited typical AIE property and relatively low thermal sensitivity (Scheme 1). We supposed that high thermal sensitivity LMOF thermometers might be obtained by embedding TPB into the framework of MOFs with the coordination effect of nitrogen atoms. In that case, all the TPB ligands would present in the same conformation to enhance the thermal sensitivity of the designed LMOFs. Meanwhile, due to the lone pair electrons of nitrogen atoms serving as coordination sites, the rotation of pyridine rings will not destroy the framework of the MOF (Scheme 1). Thus, a stable fluorescent MOF thermometer with high sensitivity and good reusability could be obtained. Herein, we revealed the rational design, synthesis, thermal sensitive property and fluorescence sensing applications of  $[\text{Cd}_2(\text{btec})(\text{TPB})_{0.5}(\text{H}_2\text{O})_4]\cdot 2\text{H}_2\text{O}$  (complex 1).

## 2. Experimental sections

### 2.1 Reagents and instruments

All reagents were commercially available and used without further purification. The powder X-ray diffraction (PXRD) tests were measured on a Bruker D8 ADVANCE X-Ray diffractometer. Elemental analyses for C, H and N were performed on a Vario EL elemental analyzer. The IR spectra were conducted on a Shimadzu IR Affinity-1S FT-IR spectrophotometer. The thermogravimetric analyses (TGA) were recorded on a Netzsch TG-209 Thermogravimetry Analyzer in  $\text{N}_2$  atmosphere. Fluorescent spectra were performed on an Agilent Cary Eclipse fluo-

rescence spectrophotometer and HITACHI fluorescence spectrophotometer (F4600).

### 2.2 Synthesis of $[\text{Cd}_2(\text{btec})(\text{TPB})_{0.5}(\text{H}_2\text{O})_4]\cdot 2\text{H}_2\text{O}$ (complex 1)

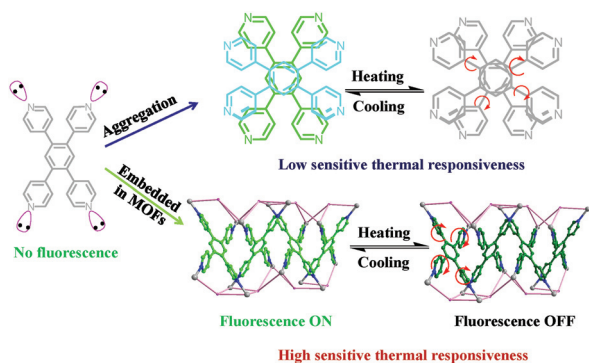
$\text{Cd}(\text{NO}_3)_2\cdot 4\text{H}_2\text{O}$  (0.019 g, 0.06 mmol),  $\text{H}_4\text{btec}$  (0.005 g, 0.02 mmol), TPB (0.004 g, 0.01 mmol), DMF (4 mL),  $\text{H}_2\text{O}$  (4 mL) and  $\text{HNO}_3$  solution (6 mol  $\text{L}^{-1}$ , 2 drops) were added to a 20 mL glass scintillation vial. The mixture was reacted at 90 °C for 2 days to yield colourless block crystals (complex 1, 81% yield based on Cd). Anal. calcd (%) for  $\text{C}_{23}\text{H}_{23}\text{O}_{14}\text{N}_2\text{Cd}_2$  (complex 1): C, 35.59; H, 2.99; N, 3.61; found: C, 35.38; H, 3.21; N, 3.36. IR (KBr)  $\nu_{\text{max}}/\text{cm}^{-1}$ : 3443 (w), 1608 (s), 1566 (m), 1484 (m), 1432 (s), 1373 (s), 826 (w), 674 (w) (Fig. S1 in the ESI†).

### 2.3 Preparation of stock solutions and working electrodes

The powder of complex 1 (2 mg) was ground and added to different solutions (2 mL). After ultrasonic dispersion for 10 minutes, homogeneous suspensions were obtained and used for the solvent screening. The powder of complex 1 (20 mg) was ground and added to water (20 mL). After ultrasonic dispersion for 30 minutes, the obtained homogeneous suspensions were used as the stock solution for further fluorescence sensing experiments. The electrolyte solution used in the photoelectric responses study was prepared with anhydrous sodium sulfate in deionized water with a concentration of 0.5 M (containing 0.1 M ascorbic acid). ITO substrates (1.5 cm × 4 cm) were washed with ethanol, acetone and water, respectively, then dried in a thermoelectric thermostat drying box at 50 °C. The powder of complex 1 (24.5 mg) was ground and added into 2.0 mL deionized water. To the above mixture was added Nafion (100  $\mu\text{L}$ ), and then the mixture was ultrasonicated for 10 min to form a suspension liquid. The working electrodes were prepared by dropping the above suspension (100  $\mu\text{L}$ ) onto the surface of the pre-treated ITO. The active coating area was controlled at about 0.5  $\text{cm}^2$ . The modified electrodes were dried in a thermoelectric thermostat drying box at 50 °C, and used as working electrodes.

### 2.4 Structure determination

Single-crystal X-ray diffraction data for complex 1 was collected on a Xcalibur Eos Gemini four-circle diffractometer with Mo  $\text{K}\alpha$  radiation ( $\lambda = 0.71073 \text{ \AA}$ ) at 173 K. Using Olex2,<sup>41</sup> the structures were solved with the ShelXS program by direct methods, and refined with the ShelXL refinement package with full-matrix least-squares minimization.<sup>42</sup> First, all of the metal atoms were located. Then, the carbon, nitrogen and hydrogen atoms were subsequently found. All of the non-hydrogen atoms were located from the initial solution and refined anisotropically. The crystallographic data for 1 is summarized in Table 1, and the selected bond lengths and angles are listed in Table S2 in the ESI.† The CCDC reference number of complex 1 is 2018947.†



**Scheme 1** Schematic illustration of the design to enhance the thermal sensitivity of TPB by embedding it into the framework of MOF.

**Table 1** Crystal data and structure refinements for complex **1**

Compound reference	<b>1</b>
Formula	C <sub>23</sub> H <sub>23</sub> N <sub>2</sub> O <sub>14</sub> Cd <sub>2</sub>
Fw.	776.23
Crystal system	Monoclinic
Space group	C2/c
<i>a</i> (Å)	27.1246(13)
<i>b</i> (Å)	13.9423(6)
<i>c</i> (Å)	13.4820(7)
$\alpha$ (°)	90
$\beta$ (°)	97.092(4)
$\gamma$ (°)	90
<i>V</i> (Å <sup>3</sup> )	5059.6(4)
<i>Z</i>	8
<i>D<sub>c</sub></i> (g cm <sup>-3</sup> )	2.038
Reflections/unique	10634/4444
<i>R</i> (int)	0.0278
GOF on <i>F</i> <sup>2</sup>	1.053
<i>R</i> <sub>1</sub> [ <i>I</i> ≥ 2σ( <i>I</i> )] <sup>a</sup>	0.0250
<i>wR</i> <sub>2</sub> [ <i>I</i> ≥ 2σ( <i>I</i> )] <sup>b</sup>	0.0544

<sup>a</sup>  $R_1 = \sum ||F_o| - |F_c|| / \sum |F_o|$ . <sup>b</sup>  $wR_2 = [\sum [w(F_o^2 - F_c^2)^2] / \sum w(F_o^2)^2]^{1/2}$ , where  $w = 1 / [2(F_o^2 + (aP)^2 + bP)]$  and  $P = (F_o^2 + 2F_c^2) / 3$ .

## 3. Results and discussion

### 3.1 Structural characterization of complex **1**

**Structural description.** Single-crystal X-ray structural analysis shows that complex **1** crystallizes in the *C2/c* space group, and possesses a complicated 3D network. The asymmetric unit of complex **1** consists of two Cd ions, one btec<sup>4-</sup> ligand, half TPB ligand, four coordinated water and two lattice water molecules. As depicted in Fig. 1a, there exist two types of coordination environments around the Cd<sup>2+</sup> ions in the crystal structure: Cd1 is seven-coordinated with an approximately pentagonal-bipyramidal coordination geometry constructed by five O atoms from three different btec<sup>4-</sup> ligands, one N1 atom from the TPB ligand and one coordinated water (O4w) molecule; Cd2 presents the same configuration as Cd1, while the difference is that it is coordinated by three O atoms from two btec<sup>4-</sup> ligands, one N2 atom from the TPB ligand and three coordinated H<sub>2</sub>O molecules (Fig. 1a). Two Cd(II) ions are bridged by two carboxylate groups in a bridging fashion to give a classical [Cd<sub>2</sub>(COO)<sub>2</sub>]<sup>2+</sup> unit with the Cd(II)⋯Cd(II) distance at about 3.838 Å, and the [Cd<sub>2</sub>(COO)<sub>2</sub>]<sup>2+</sup> unit can be simplified into a five-connected node. The btec<sup>4-</sup> ligand adopts two different coordination modes: the first kind of btec<sup>4-</sup> ligand is coordinated with four Cd<sup>2+</sup> ions with two carboxylate groups in the μ<sup>2</sup>-η<sup>2</sup>:η<sup>1</sup> mode, and the second kind of btec<sup>4-</sup> ligand is coordinated with six Cd<sup>2+</sup> ions with four carboxylate groups in the μ<sup>1</sup>-η<sup>1</sup>:η<sup>1</sup> and μ<sup>2</sup>-η<sup>2</sup>:η<sup>1</sup> modes (Fig. 1b). If the TPB ligand and two-coordinated btec<sup>4-</sup> ligands are neglected, each six-coordinated btec<sup>4-</sup> ligand acts as a μ<sub>4</sub>-bridging ligand, linking four [Cd<sub>2</sub>(COO)<sub>2</sub>]<sup>2+</sup> units to build a 2D layer structure in the *ac* plane (Fig. 1c). On the basis of this conductive way, these neighbouring 2D layers are further connected by four-coordinated TPB ligands and two-coordinated btec<sup>4-</sup> ligands to form a complicated 3D network (Fig. 1d and e).

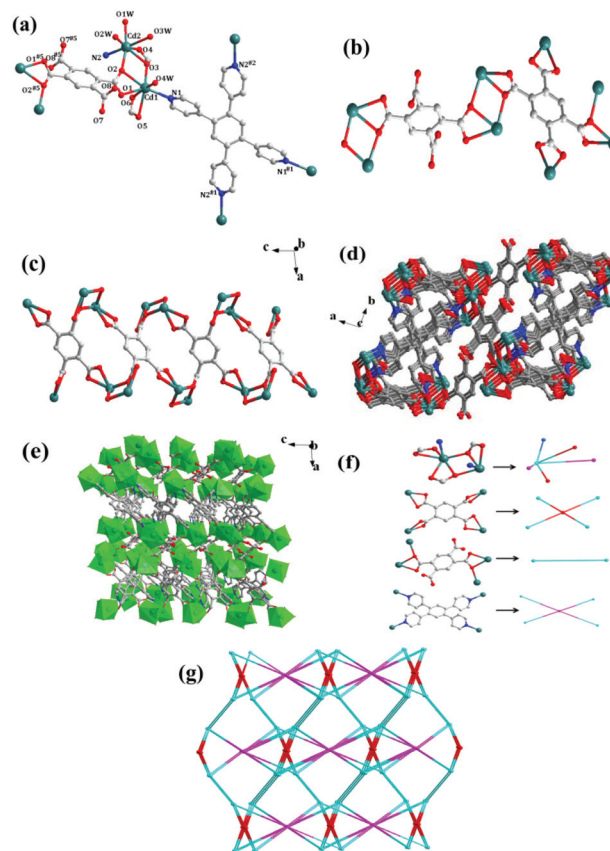


**Fig. 1** (a) The coordination environment of Cd(II) ions with hydrogen atoms and lattice water molecules omitted for clarity. Symmetry code: #1  $1 - x, -1 - y, -z$ ; #2  $+x, -1 - y, 1/2 + z$ ; #3  $1 - x, -y, -z$ ; #4  $+x, -1 - y, -1/2 + z$ ; #5  $1/2 - x, -1/2 - y, -z$ ; (b) the coordination mode of btec<sup>4-</sup> ligands; (c) the layer structure constructed by the [Cd<sub>2</sub>(COO)<sub>2</sub>]<sup>2+</sup> unit and btec<sup>4-</sup> ligands; (d) the layers are further connected by TPB ligand and two-coordinated btec<sup>4-</sup> ligands to form a 3D framework; (e) 3D structure viewed along the *b* axis; (f) defined 5-connected nodes of [Cd<sub>2</sub>(COO)<sub>2</sub>]<sup>2+</sup>, 2- and 4-connected nodes of btec<sup>4-</sup> and 4-connected nodes of TPB; cyan balls represent the [Cd<sub>2</sub>(COO)<sub>2</sub>]<sup>2+</sup> units, red balls represent the center of the btec<sup>4-</sup> ligands and the pink balls represent the center of TPB; (g) topological view showing the equivalent 3D framework for complex **1** along the *c* axis.

In addition, from a topological point of view, each [Cd<sub>2</sub>(COO)<sub>2</sub>]<sup>2+</sup> unit can be considered as a 5-connected node, the tpb ligands and btec<sup>4-</sup> ligands can be regarded as 4-connecting nodes, respectively (Fig. 1f). Therefore, such supramolecular framework can be simplified as a (4,5)-connected net with the Schläfli symbol of (4<sup>4</sup>·6<sup>2</sup>) (4<sup>3</sup>·6<sup>2</sup>·7<sup>2</sup>·8<sup>3</sup>)<sub>2</sub> (4<sup>2</sup>·8<sup>4</sup>) analysed by the TOPOS program (Fig. 1f and g).<sup>43,44</sup>

**PXRD analysis.** The phase purity of the as-synthesized complex **1** was confirmed by X-ray powder diffraction (XRD) measurements. As shown in Fig. 4c, the PXRD pattern of the as-synthesized complex **1** (the red line) matches well with the simulated one based on the single-crystal diffraction data, which revealed the good purity of complex **1**.

**TG analysis.** Thermogravimetric measurement for complex **1** was carried out from room temperature to 790 °C under N<sub>2</sub>

atmosphere. As shown in Fig. S2,† the TG curve of complex 1 shows a weight loss of 11.6% from room temperature to 330 °C, which corresponds to the removal of the lattice and coordinated water molecules (calcd 13.9%). The discrepancy between the found and theoretical values could be attributed to the loss of the lattice water at room temperature. The desolvated framework starts to collapse upon further heating.

### 3.2 Thermosensitive property of complex 1

Initially, in order to reveal the fluorescence property of complex 1 at room temperature, the solid state fluorescence spectra of complex 1 and TPB were recorded and are displayed in Fig. 2a. Complex 1 exhibited a characteristic fluorescence emission centered at 390 nm upon excitation at 300 nm (Fig. 2a, the red line). TPB displayed a similar emission with complex 1, but the maximum emission was centered at 360 nm (Fig. 2a, the blue line). The remarkable red shift (about 30 nm) of complex 1 compared with that of TPB could be attributed to the effects of the ligand–metal coordination interactions.<sup>4,45</sup> In addition, photographs of complex 1 after heating and cooling under 254 nm UV lamp were recorded and are displayed in Fig. 2b. Apparently, the fluorescence emission intensity sharply decreased with the ambient temperature change from 20 °C to 180 °C. The above phenomenon revealed that the fluorescence emission property of complex 1 is closely related to the ambient temperature.

To further reveal the thermo-sensitive property, the fluorescence spectra of complex 1 were recorded with the ambient temperature slowly changed from 160 °C to 20 °C. As shown in Fig. 3a, the fluorescence intensity gradually increased with the ambient temperature change from 160 °C to 20 °C (the fluorescence intensities of complex 1 centered at 390 nm were recorded, and are displayed in Fig. S3†). Correspondingly, the fluorescence quenching efficiency<sup>46</sup> of complex 1 changed from 20 °C to 160 °C, and was calculated and displayed in

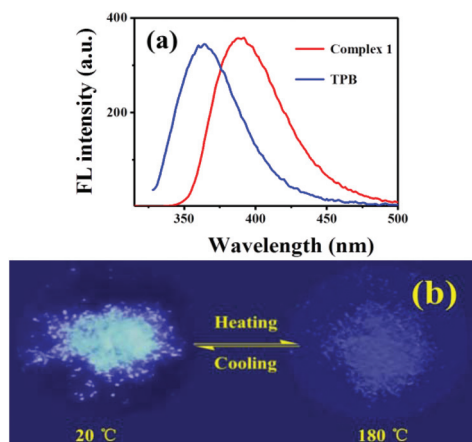


**Fig. 2** (a) Solid state fluorescence spectra of complex 1 and TPB ( $\lambda_{\text{ex}} = 300$  nm); (b) photograph of complex 1 at 20 °C and 180 °C under a 254 nm luminescent lamp.

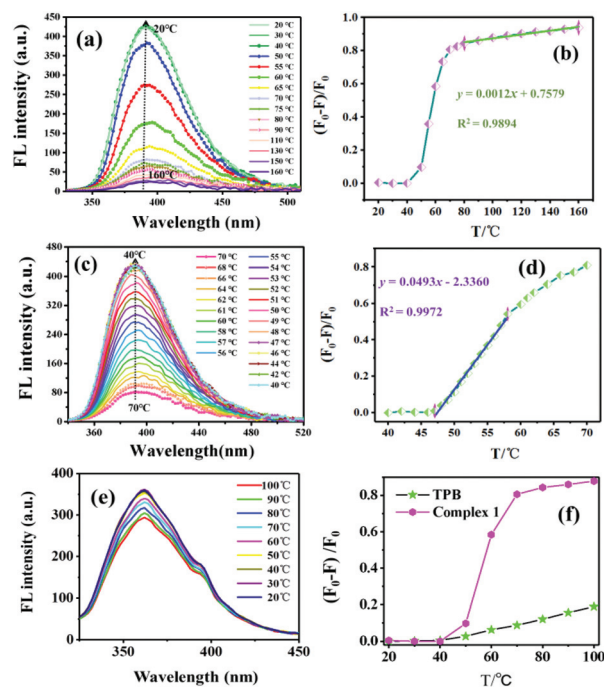


**Fig. 3** (a) Solid state fluorescence spectra of complex 1 with gradual change in temperature from 160 °C to 20 °C ( $\lambda_{\text{ex}} = 300$  nm, slits: 2.5 nm/5 nm); (b) fluorescence quenching efficiency of complex 1 calculated with temperature changes from 160 °C to 20 °C ( $F_0$  is the fluorescence intensity of complex 1 at 20 °C and  $F$  is the fluorescence intensity of complex 1 changed with temperature variation,  $\lambda_{\text{em}} = 390$  nm); (c) fluorescence spectra of complex 1 with gradual temperature changes from 70 °C to 40 °C ( $\lambda_{\text{ex}} = 300$  nm, slits: 2.5 nm/5 nm); (d) fluorescence quenching efficiency of complex 1 ( $\lambda_{\text{em}} = 390$  nm) with temperature changes from 70 °C to 40 °C; (e) fluorescence spectra of TPB recorded with gradual temperature changes from 100 °C to 20 °C; (f) fluorescence quenching efficiency of TPB and complex 1 in the temperature range from 20 °C to 100 °C.

Fig. 3b. Interestingly, complex 1 displayed an obvious thermal responsiveness at temperatures ranging from 40 °C to 160 °C, as illustrated in Fig. 3b. A good linear relationship between the fluorescence quenching efficiency and the ambient temperature was observed in the temperature range from 80 °C to 160 °C. The linear equation was determined to be  $y = 0.0012x + 0.7579$  (Fig. 3b,  $R^2 = 0.9894$ , where  $y$  represents the fluorescence quenching efficiency and  $x$  represents the ambient temperature). It is noteworthy that the fluorescence quenching efficiency changed dramatically from 40 °C to 70 °C. In order to reveal the thermal responsiveness in detail, the fluorescence spectra of complex 1 were recorded with slow changes in the ambient temperature from 70 °C to 40 °C (Fig. 3c and d).

As shown in Fig. 3c and Fig. S4,† the fluorescence intensity of complex 1 dramatically changed with the variation of temperature, especially in the range from 47 °C to 70 °C (with good structural stability and Fig. S7†). Interestingly, a good linear relationship of the quenching efficiency against the temperature over the range from 47 °C to 58 °C was observed (Fig. 3d,  $y = 0.0493x - 2.3360$ ,  $R^2 = 0.9972$ , where  $y$  represents the fluorescence quenching efficiency and  $x$  represents the ambient

temperature). All of the above results revealed that complex **1** has high thermal sensitivity.

**Plausible mechanism for the sensitive thermal responsiveness.** For comparison, the fluorescence spectra of TPB were recorded with gradually changing temperature from 100 °C to 20 °C. As displayed in Fig. 3e, the fluorescence intensity of TPB slowly increased with decreasing ambient temperature. The fluorescence quenching efficiency of TPB and complex **1** in the temperature range from 20 °C to 100 °C are displayed in Fig. 3f. Apparently, the fluorescence quenching efficiency of complex **1** sharply increased to 88% when the ambient temperature reached 100 °C, while the fluorescence quenching efficiency of the TPB ligand is below 20% at that temperature. Thus, complex **1** is much more sensitive to the ambient temperature variation than the TPB ligands.

A possible mechanism to rationalize these results is proposed in Scheme 2. When AIE molecules such as TPB are embedded into MOFs, a specific and uniform configuration would be obtained. Compared with the free TPB ligands, the uniformed TPB ligand in the framework is easier to rotation/vibration when the ambient temperature changed. The enhanced rotation/vibration of TPB will change the radiative/nonradiative decay rate and lead to the fluorescence intensity variation. This may explain the sharp fluorescence quenching of complex **1** with increasing temperature (Fig. 3a). Thus, the above control experiments could prove our assumption that the thermo-sensitivity of the AIE molecules could be enhanced by embedding into MOFs to form a uniform and particular configuration, just as the proverb goes “united we stand, divided we fall” (Scheme 2).

### 3.3 Fluorescence sensing property of complex **1** in solvents

**Solvent screening.** Initially, complex **1** was dispersed in various solvents to screen the optimized dispersion medium for further fluorescence sensing application. The fluorescence spectra of complex **1** after dispersion in different solvents were recorded, and are displayed in Fig. 4a. Relatively stable suspensions were obtained in most of the solvents, and good fluorescence emissions were observed ( $\lambda_{\text{ex}} = 300$  nm,  $\lambda_{\text{em}} = 390$  nm). Interestingly, the maximum emission of complex **1** shifted to 410 nm after dispersion in water. However, no obvious emission shift was observed when other solvents were used as the dispersion medium. Moreover, the fluorescence

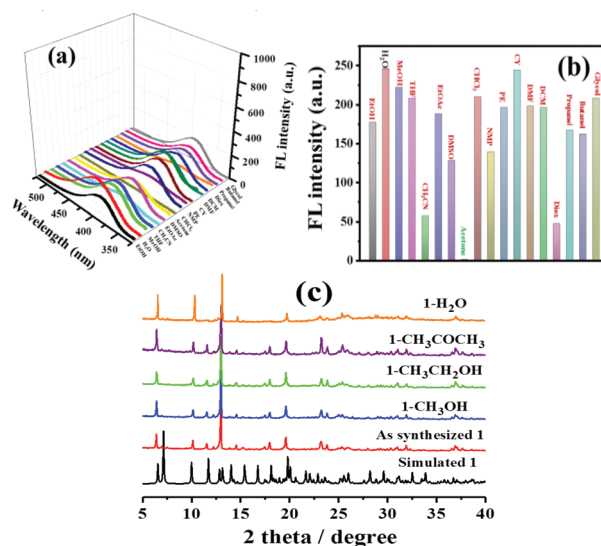


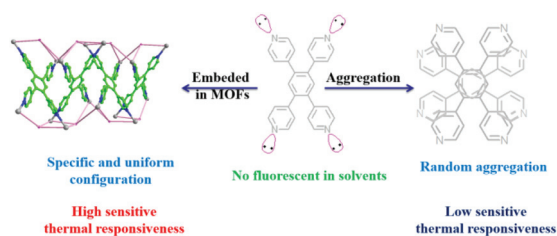
**Fig. 4** (a) Fluorescence spectra of complex **1** after dispersion in different solvents ( $\lambda_{\text{ex}} = 300$  nm, slits: 5 nm/5 nm); (b) fluorescence emission intensities of complex **1** suspension ( $\lambda_{\text{em}} = 410$  nm in water,  $\lambda_{\text{em}} = 390$  nm in other solvents); (c) PXRD patterns of complex **1** before and after dispersion in solvents (water, acetone, ethanol and methanol).

intensity of the above suspensions centered at 390 nm ( $\lambda_{\text{em}} = 410$  nm in water) was recorded.

As illustrated in Fig. 4b, complex **1** exhibited good emission in most of the tested solvents, such as ethanol, methanol, water, dichloromethane (DCM), ethyl acetate (EtOAc), and others. Thus, complex **1** could be used in both aqueous and organic dispersion mediums. Also worthy of mention is that complex **1** displayed the maximum emission in water, which could facilitate the detection of contamination in water. Interestingly, the fluorescence emission of complex **1** was completely quenched when acetone was used as the dispersion medium. Therefore, complex **1** might be used in the fluorescence detection of acetone in water. In order to reveal the stability of complex **1** in various solvents, PXRD patterns of complex **1** that were filtered from solvents such as ethanol, methanol, water and acetone were recorded, and are displayed in Fig. 4c. Delightfully, the PXRD patterns of the recovered complex **1** matched well with the simulated one based on the single-crystal diffraction data, which revealed the good stability of complex **1** in various solvents (Fig. 4c).

**Fluorescence distinguishes D<sub>2</sub>O from H<sub>2</sub>O.** To further reveal the fluorescence property of the complex 1-H<sub>2</sub>O suspension, the fluorescence spectra of complex **1** were recorded at different times after dispersion in water. As illustrated in Fig. 5a, a big red shift (from 390 nm to 410 nm) was observed in less than 1 minute in the emission spectra of complex **1**. The fluorescence intensity of the complex 1-H<sub>2</sub>O suspension reached a stable value in less than 1.5 minutes (Fig. 5b). To our delight, the fluorescence intensity of this suspension centered at 410 nm has no obvious change after dispersion for one hour (Fig. 5b).

Moreover, a control experiment was carried out by using D<sub>2</sub>O as the dispersion medium. As displayed in Fig. 5c, the



**Scheme 2** A plausible mechanism for enhancement of the thermal sensitivity of TBP.

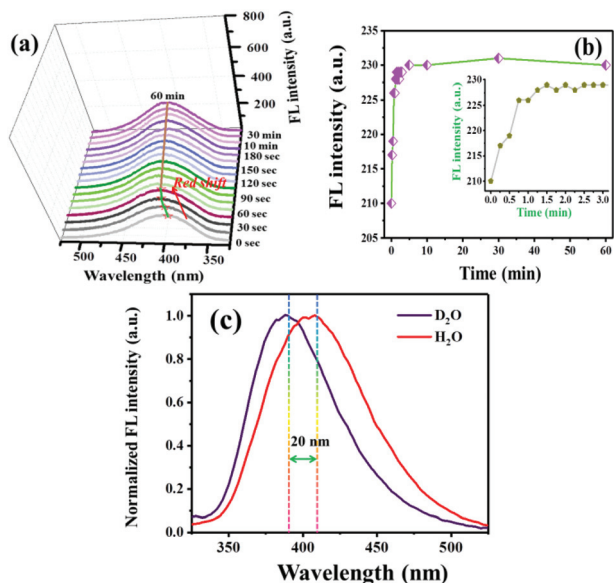


**Fig. 5** (a) Fluorescence spectra of complex **1** after dispersion in de-ionized water for different times (from 0 to 60 minutes,  $\lambda_{\text{ex}} = 300$  nm, slits: 5 nm/5 nm); (b) fluorescence intensities of the complex **1**-H<sub>2</sub>O suspension (centered at 410 nm) with the time changed from 0 to 60 minutes; (c) fluorescence spectra of complex **1** after dispersion in H<sub>2</sub>O and D<sub>2</sub>O ( $\lambda_{\text{ex}} = 300$  nm, slits: 5 nm/5 nm).

maximum emission wavelength of complex **1** emerged at 390 nm when D<sub>2</sub>O was used as the dispersion medium. A remarkable blue shift (about 20 nm) in the fluorescence emission spectrum of complex **1** was observed when D<sub>2</sub>O was used as the dispersion medium compared with that in H<sub>2</sub>O, which could be used for distinguishing D<sub>2</sub>O from H<sub>2</sub>O.

**Fluorescent detection of acetone in water.** Inspired by the above results, the fluorescence detection of acetone in water was carried out by the gradual addition acetone to the complex **1**-H<sub>2</sub>O suspension (3 mL), and the fluorescence spectra were recorded. As shown in Fig. 6a, the fluorescence of the complex **1**-H<sub>2</sub>O suspension was gradually quenched with the addition of acetone. A noticeable fluorescence decrease could be observed after the addition of 2  $\mu\text{L}$  acetone (0.06%, vol%),

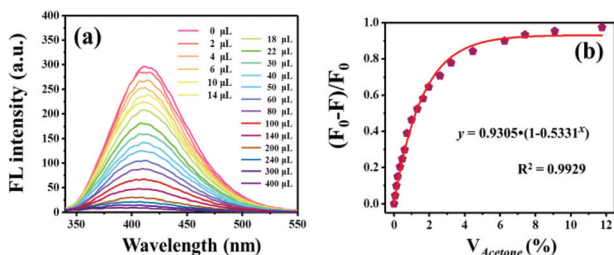


**Fig. 6** (a) Fluorescence spectra of the complex **1**-H<sub>2</sub>O suspension (3 mL) with the gradual addition of acetone from 0  $\mu\text{L}$  to 400  $\mu\text{L}$  ( $\lambda_{\text{ex}} = 300$  nm,  $\lambda_{\text{em}} = 410$  nm, slits: 5 nm/10 nm); (b) fluorescence quenching efficiency of the complex **1**-H<sub>2</sub>O suspension after addition of acetone ( $\lambda_{\text{ex}} = 300$  nm,  $\lambda_{\text{em}} = 410$  nm, slits: 5 nm/10 nm).

which indicated that the complex **1**-H<sub>2</sub>O suspension could be used in the highly sensitive sensing of acetone in water.<sup>47–49</sup>

Fluorescence intensities of the complex **1**-H<sub>2</sub>O suspension with acetone centered at 410 nm were recorded, and are displayed in Fig. S5.† In order to evaluate the performance of complex **1** in the fluorescence sensing of acetone in water, the fluorescence quenching efficiency  $((F_0 - F)/F_0)^{46}$  was calculated with the gradual addition of acetone. As shown in Fig. 6b, the fluorescence quenching efficiency of the complex **1**-H<sub>2</sub>O suspension gradually increased with the addition of acetone. It is interesting to note that the fluorescence quenching efficiency reached 65% and 85% with 1.9% (vol%) and 4.5% (vol%) acetone, respectively. Moreover, the fluorescence quenching efficiency fitted well with the following non-linear equation:  $y = 0.9305 \cdot (1 - 0.5331^x)$  ( $R^2 = 0.9929$ , where  $y$  represents the fluorescence quenching efficiency and  $x$  represents the volume ratio of acetone), which revealed the good potential of complex **1** in the quantitative detection of acetone in water.

In addition, the mechanism for the fluorescence quenching sensing of acetone could be ascribed to the strong inner filtering effect (IFE) between complex **1** and acetone. As can be seen from the UV-Vis spectrum of acetone, the absorption of acetone lies in the range of 200 nm–325 nm, which could overlap with the excitation spectrum of complex **1** (ranging from 220 nm to 300 nm, Fig. S6a and b†). The light (300 nm) used for excitation would be competitively absorbed by acetone after the addition of acetone to the complex **1** water suspension, which would lead to the sharp fluorescence quenching of complex **1**. Furthermore, the inner filtering effect (IFE) between complex **1** and acetone could be confirmed by the overlap between the UV-Vis absorption of complex **1** and acetone (Fig. S6c†).

### 3.4 Photoelectric responses

Photoactive metal–organic frameworks (MOFs) are promising candidate materials that could be used in the photocatalytic hydrogen production<sup>50,51</sup> and sensing,<sup>52,53</sup> among others. In order to reveal the photoelectronic performance of complex **1**, the photocurrent-time relationship of complex **1** was recorded

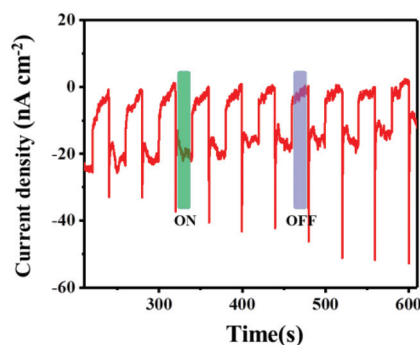


**Fig. 7** Transient current density-time curves of the complex **1** modified electrode in 0.5 M Na<sub>2</sub>SO<sub>4</sub> without bias potential (every on–off cycle lasts for 20 seconds).

using a standard three-electrode system with a platinum electrode as the reference electrode and an AgCl/Ag electrode as the reference electrode. The preliminary testing result is displayed in Fig. 7. To our delight, the complex **1**-modified electrode yielded steady photocurrents in the absence of a bias potential when the light source was turned on. The average photocurrent density observed on the working electrode was found to be 30 nA cm<sup>-2</sup>. Moreover, the photocurrent density of the complex **1**-modified electrode has no obvious decrease after the test was performed for 600 seconds (every on-off cycle last for 20 seconds). Therefore, the above preliminary results indicated that complex **1** might be modified and used as a photoelectric material in the future.

## 4. Conclusions

By embedding TPB into the framework of MOFs, a novel thermo-sensitive Cd-MOF fluorescent probe (complex **1**) has been rationally designed and constructed. A highly sensitive thermal responsiveness was observed in a wide temperature range from 20 °C to 160 °C. Good linear relationships were obtained between the fluorescence quenching efficiency of complex **1** and the circumstance temperature, revealing the good potential of complex **1** to be used as a quantitative fluorescence thermometer. A big red shift emission was observed when complex **1** was dispersed in H<sub>2</sub>O compared with D<sub>2</sub>O, which could be used in distinguishing D<sub>2</sub>O from H<sub>2</sub>O *via* fluorescence. Stable complex **1**-H<sub>2</sub>O suspensions were obtained and used in the real-time sensing of acetone in water with an experimental detection limit of 0.06% (vol%). Moreover, a steady photocurrent was observed for the complex **1** modified electrode in the absence of a bias potential, indicating that complex **1** might be modified and used as a photoelectric material in the future. In addition, the proposed method could be used for the preparation of interesting thermo-sensitive fluorescent MOFs probes in the future.

## Author contributions

Ping Ju: Data curation and writing-original draft. Mengting Li: data curation. Hua Yang: data curation. Long Jiang: software. Lian Xia: formal analysis. Rongmei Kong: methodology. Ensheng Zhang: data curation and investigation. Fengli Qu: supervision.

## Conflicts of interest

There are no conflicts to declare.

## Acknowledgements

This work was financially supported by the National Natural Science Foundation of China (22007055, 21775089, 22074080),

Natural Science Foundation of Shandong Province of China (ZR2020QB156), Changjiang Scholar Program of the Ministry of Education of China (Q2019258), Taishan Scholar Program of Shandong Province (tsqn201909106), and the Startup Foundation for Doctors of Qufu Normal University.

## Notes and references

- 1 Y. Li, A. S. Xiao, B. Zou, H. X. Zhang, K. L. Yan and Y. Lin, Advances of metal-organic frameworks for gas sensing, *Polyhedron*, 2018, **154**, 83–97.
- 2 M. D. Allendorf, C. A. Bauer, R. K. Bhakta and R. J. T. Houk, Luminescent metal-organic frameworks, *Chem. Soc. Rev.*, 2009, **38**, 1330–1352.
- 3 Y. J. Cui, B. L. Chen and G. D. Qian, Lanthanide metal-organic frameworks for luminescent sensing and light-emitting applications, *Coord. Chem. Rev.*, 2014, **273**, 76–86.
- 4 Y. M. Zhang, S. Yuan, G. Day, X. Wang, X. Y. Yang and H. C. Zhou, Luminescent sensors based on metal-organic frameworks, *Coord. Chem. Rev.*, 2018, **354**, 28–45.
- 5 K. Pawan, A. Deep and K. H. Kim, Metal organic frameworks for sensing applications, *TrAC, Trends Anal. Chem.*, 2015, **73**, 39–53.
- 6 P. Mahata, S. K. Mondal, D. K. Singha and P. Majee, Luminescent rare-earth-based MOFs as optical sensors, *Dalton Trans.*, 2017, **46**, 301–328.
- 7 J. P. Lei, R. C. Qian, P. H. Ling, L. Cui and H. X. Ju, Design and sensing applications of metal-organic framework composites, *TrAC, Trends Anal. Chem.*, 2014, **58**, 71–78.
- 8 S. Homayoonnia and S. Zeinali, Design and fabrication of capacitive nanosensor based on MOF nanoparticles as sensing layer for VOCs detection, *Sens. Actuators, B*, 2016, **237**, 776–786.
- 9 D. Tian, Y. Li, R. Y. Chen, Z. Chang, G. Y. Wang and X. H. Bu, A luminescent metal-organic framework demonstrating ideal detection ability for nitroaromatic explosives, *J. Mater. Chem. A*, 2014, **2**, 1465–1470.
- 10 F. Y. Zhong, X. Zhang, C. Q. Zheng, H. Xu, J. K. Gao and S. Q. Xu, A fluorescent titanium-based metal-organic framework sensor for nitroaromatics and nanomolar Fe<sup>3+</sup> detection, *J. Solid State Chem.*, 2020, 121391.
- 11 L. L. Zhang, Z. X. Kang, X. L. Xin and D. F. Sun, Metal-organic frameworks based luminescent materials for nitroaromatics sensing, *CrystEngComm*, 2016, **18**, 193–206.
- 12 H. Wang, W. T. Yang and Z. M. Sun, Mixed-ligand Zn-MOFs for highly luminescent sensing of nitro compounds, *Chem. – Asian J.*, 2013, **8**, 982–989.
- 13 P. C. Xing, D. Wu, J. S. Chen, J. M. Song, C. J. Mao, Y. H. Gao and H. L. Niu, A Cd-MOF as a fluorescent probe for highly selective, sensitive and stable detection of antibiotics in water, *Analyst*, 2019, **144**, 2656–2661.
- 14 Z. H. Jiao, X. L. Jiang, S. L. Hou, M. H. Tang and B. Zhao, Highly sensitive and selective luminescence sensor based on two fold interpenetrated MOFs for detecting glutamate in serum, *Inorg. Chem.*, 2020, **59**, 2171–2177.

- 15 A. M. Walker, B. Civalieri, B. Slater, C. Mellot-Draznieks, F. Corà, C. M. Zicovich-Wilson, G. Román-Pérez, J. M. Soler and J. D. Gale, Flexibility in a metal-organic framework material controlled by weak dispersion forces: the bistability of MIL-53(Al)\*\*, *Angew. Chem.*, 2010, **122**, 7663–7665.
- 16 A. Schneemann, V. Bon, I. Schwedler, I. Senkovska, S. Kaskel and R. A. Fischer, Flexible metal-organic frameworks, *Chem. Soc. Rev.*, 2014, **43**, 6062–6096.
- 17 Z. Chang, D. H. Yang, J. Xu, T. L. Hu and X. H. Bu, Flexible metal-organic frameworks: recent advances and potential applications, *Adv. Mater.*, 2015, **27**, 5432–5441.
- 18 A. Clearfield, Flexible MOFs under stress: pressure and temperature, *Dalton Trans.*, 2016, **45**, 4100–4112.
- 19 M. J. Kalmutzki, C. S. Diercks and O. M. Yaghi, Metal-organic frameworks for water harvesting from air, *Adv. Mater.*, 2018, **30**, 1704304.
- 20 Y. Li, Temperature and humidity sensors based on luminescent metal-organic frameworks, *Polyhedron*, 2020, **179**, 114413.
- 21 Z. P. Wang, S. S. Yu, H. Zhang and H. B. Duan, Thermochromic luminescence and dielectric response of copper(i) iodide based MOFs as luminescent thermometer, *Synth. Met.*, 2019, **255**, 116104.
- 22 M. L. Shen, L. Xu, B. Liu, H. Jiao and Y. U. Kwon, Thermosensitive fluorescent Eu-based metal-organic framework and its polyether sulfone composite film as thermal sensor, *Dalton Trans.*, 2018, **47**, 8330–8336.
- 23 Y. Yang, Y. Z. Wang, Y. Feng, X. R. Song, C. Cao, G. L. Zhang and W. S. Li, Three isostructural Eu<sup>3+</sup>/Tb<sup>3+</sup> co-doped MOFs for wide-range ratiometric temperature sensing, *Talanta*, 2020, **208**, 120354.
- 24 Y. Hasegawa and Y. Kitagawa, Thermo-sensitive luminescence of lanthanide complexes, clusters, coordination polymers and metal-organic frameworks with organic photosensitizers, *J. Mater. Chem. C*, 2019, **7**, 7494–7511.
- 25 D. Zhao, D. Yue, K. Jiang, L. Zhang and C. X. Li, Isostructural Tb<sup>3+</sup>/Eu<sup>3+</sup> Co-doped metal-organic framework based on pyridine-containing dicarboxylate ligands for ratiometric luminescence temperature sensing, *Inorg. Chem.*, 2019, **58**, 2637–2644.
- 26 F. X. Coudert, Responsive metal-organic frameworks and framework materials: under pressure, taking the heat, in the spotlight, with friends, *Chem. Mater.*, 2015, **27**, 1905–1916.
- 27 Y. Wu, A. Kobayashi, G. J. Halder, V. K. Peterson, K. W. Chapman, N. Lock, P. D. Southon and C. J. Kepert, Negative thermal expansion in the metal-organic framework material Cu<sub>3</sub>(1,3,5-benzenetri carboxylate)<sub>2</sub>, *Angew. Chem. Int. Ed.*, 2008, **47**, 8929–8932.
- 28 Y. Wu, V. K. Peterson, E. Luks, T. A. Darwish and C. J. Kepert, Interpenetration as a mechanism for negative thermal expansion in the metal-organic framework Cu<sub>3</sub>(btb)<sub>2</sub>(MOF-14), *Angew. Chem.*, 2014, **126**, 5275–5278.
- 29 L. Zhang, X. F. Kuang, X. Y. Wu, W. B. Yang and C. Z. Lu, Supramolecular interactions induced hinge-like motion of a metal-organic framework accompanied by anisotropic thermal expansion, *Dalton Trans.*, 2014, **43**, 7146–7152.
- 30 Y. Liu, J. H. Her, A. Dailly, A. J. Ramirez-Cuesta, D. A. Neumann and C. M. Brown, Reversible structural transition in MIL-53 with large temperature hysteresis, *J. Am. Chem. Soc.*, 2008, **130**, 11813–11818.
- 31 T. D. Bennett, D. A. Keen, J. C. Tan, E. R. Barney, A. L. Goodwin and A. K. Cheetham, Thermal amorphization of zeolitic imidazolate frameworks, *Angew. Chem.*, 2011, **123**, 3123–3127.
- 32 X. S. Hu, X. B. Lou, C. Li, Q. Chen, Q. Yang and B. W. Hu, Amorphization and disordering of metal-organic framework materials for rechargeable batteries by thermal treatment, *New J. Chem.*, 2017, **41**, 6415–6419.
- 33 Y. Yang, L. Chen, F. L. Jiang, M. X. Yu, X. Y. Wan, B. Zhang and M. C. Hong, A family of doped lanthanide metal-organic frameworks for wide-range temperature sensing and tunable white light emission, *J. Mater. Chem. C*, 2017, **5**, 1981–1989.
- 34 Y. Cui, R. Song, J. Yu, M. Liu, Z. Wang, C. Wu, Y. Yang, Z. Wang, B. Chen and G. Qian, Dual-emitting MOF ⊃ Dye composite for ratiometric temperature sensing, *Adv. Mater.*, 2015, **27**, 1420–1425.
- 35 T. Xia, T. Song, Y. Cui, Y. Yang and G. Qian, A dye encapsulated terbium-based metal-organic framework for ratiometric temperature sensing, *Dalton Trans.*, 2016, **45**, 18689–18695.
- 36 N. L. C. Leung, N. Xie, W. Z. Yuan, Y. Liu, Q. Y. Wu, Q. Peng, Q. Miao, J. W. Y. Lam and B. Z. Tang, Restriction of intramolecular motions: the general mechanism behind aggregation-induced emission, *Chem. – Eur. J.*, 2014, **20**, 1–6.
- 37 Y. C. Chen, J. W. Y. Lam, R. T. K. Kwok, B. Liu and B. Z. Tang, Aggregation-induced emission: fundamental understanding and future developments, *Mater. Horiz.*, 2019, **6**, 428–433.
- 38 J. Liang, B. Z. Tang and B. Liu, Specific light-up bioprobes based on AIEgen conjugates, *Chem. Soc. Rev.*, 2015, **44**, 2798–2811.
- 39 Q. Zeng, Z. Li, Y. Q. Dong, C. A. Di, A. J. Qin, Y. N. Hong, L. Ji, Z. C. Zhu, C. K. W. Jim, G. Yu, Q. Q. Li, Z. A. Li, Y. Q. Liu, J. G. Qin and B. Z. Tang, Fluorescence enhancements of benzene-cored luminophors by restricted intramolecular rotations: AIE and AIEE effects, *Chem. Commun.*, 2007, **1**, 70–72.
- 40 E. S. Zhang, X. F. Hou, Z. Zhang, Y. Q. Zhang, J. J. Wang, H. Yang, J. M. You and P. Ju, A novel biomass-based reusable AIE material: AIE properties and potential applications in amine/ammonia vapor sensing and information storage, *J. Mater. Chem. C*, 2019, **7**, 8404–8411.
- 41 O. V. Dolomanov, L. J. Bourhis, R. J. Gildea, J. A. K. Howard and H. Puschmann, OLEX2: a complete structure solution, refinement and analysis program, *J. Appl. Crystallogr.*, 2009, **42**, 339–341.
- 42 G. M. Sheldrick, A short history of SHELX, *Acta Crystallogr.*, 2008, **A64**, 112–122.
- 43 V. A. Blatov, Multipurpose crystallochemical analysis with the program package TOPOS, *Int. Union Crystallogr., Comm. Crystallogr. Comput. Newsl.*, 2006, **7**, 4–38.

- 44 L. Öhrström and K. Larsson, *Molecule Based Materials: The Structural Network Approach*, Elsevier, Amsterdam, 2005, pp. 151–325.
- 45 Y. L. Wu, G. P. Yang, Y. Q. Zhao, W. P. Wu, B. Liu and Y. Y. Wang, Three new solvent-directed Cd(II)-based MOFs with unique luminescent properties and highly selective sensors for Cu<sup>2+</sup> cations and nitrobenzene, *Dalton Trans.*, 2015, **44**, 3271–3277.
- 46 P. Ju, E. S. Zhang, L. Jiang, Z. Zhang, X. Y. Hou, Y. Q. Zhang, H. Yang and J. J. Wang, A novel microporous Tb-MOF fluorescent sensor for highly selective and sensitive detection of picric acid, *RSC Adv.*, 2018, **8**, 21671–21678.
- 47 T. Gao, B. X. Dong, Y. Sun, W. L. Liu and Y. L. Teng, Fabrication of a water-stable luminescent MOF with an open Lewis basic triazolyl group for the high-performance sensing of acetone and Fe<sup>3+</sup> ions, *J. Mater. Sci.*, 2019, **54**, 10644–10655.
- 48 Q. S. Zhang, J. Wang, A. M. Kirillov, W. Dou, C. Xu, C. L. Xu, L. Z. Yang, R. Fang and W. S. Liu, Multifunctional Ln-MOF luminescent probe for efficient sensing of Fe<sup>3+</sup>, Ce<sup>3+</sup>, and acetone, *ACS Appl. Mater. Interfaces*, 2018, **10**, 23976–23986.
- 49 N. Goel and N. Kumarc, A dual-functional luminescent Tb (III) metal-organic framework for the selective sensing of acetone and TNP in water, *RSC Adv.*, 2018, **8**, 10746–10755.
- 50 Y. P. Zhu, J. Yin, E. Abou-Hamad, X. K. Liu, W. Chen, T. Yao, O. F. Mohammed and H. N. Alshareef, Highly stable phosphonate-based MOFs with engineered bandgaps for efficient photocatalytic hydrogen production, *Adv. Mater.*, 2020, 1906368.
- 51 H. Liu, C. Y. Xu, D. D. Li and H. L. Jiang, Photocatalytic hydrogen production coupled with selective benzylamine oxidation over MOF composites, *Angew. Chem.*, 2018, **130**, 5477–5481.
- 52 Y. Cao, L. N. Wang, C. Y. Wang, X. Y. Hu, Y. L. Liu and G. X. Wang, Sensitive detection of glyphosate based on a Cu-BTC MOF/g-C<sub>3</sub>N<sub>4</sub> nanosheet photoelectrochemical sensor, *Electrochim. Acta*, 2019, **317**, 341–347.
- 53 X. J. Liao, H. M. Fu, T. T. Yan and J. P. Lei, Electroactive metal-organic framework composites: Design and biosensing application, *Biosens. Bioelectron.*, 2019, **146**, 111743.